Title

Projection-defined ventral tegmental area neurons exhibit fentanyl-induced molecular and functional adaptations that differentially support drug-context associations

Authors

Annalisa Montemarano[1], Hajra Sohail[1], Logan D. Fox[1], Laura B. Murdaugh[1], Alexandria E. Ostman[1], Samiksha Pandey[1], Kyrsten Derr[1], Megan E. Fox[1,2,3]

1. Department of Anesthesiology and Perioperative Medicine, Pennsylvania State University College of Medicine, Hershey PA
2. Department of Neuroscience and Experimental Therapeutics, Pennsylvania State University College of Medicine, Hershey PA
3. Address correspondence to Megan E. Fox

   500 University Drive

   C2850, MC #H187

   Hershey, PA 17033

   Tel:717-531-0003 x289635

   mfox@psu.edu

ABSTRACT

Opioid use disorder (OUD) remains a major public health concern affecting millions of individuals, with potent synthetic opioids driving overdose deaths. To advance OUD treatment, it is necessary to improve understanding of how synthetic opioids impact the brain and promote persistent use. The ventral tegmental area (VTA) sends diverse projections to several regions including nucleus accumbens (NAc) and prefrontal cortex (PFC), and is critical for opioid reward. Previous work shows downstream projection target influences baseline properties and opioid-induced neuroadaptations in VTA, but most work has focused on natural opioids and single neurotransmitter-defined cell-types. As such, there is limited understanding of how diverse VTA cell-types function together to mediate drug-directed behaviors through their shared circuit outputs. Here, we investigate how projection-defined VTA neurons exhibit differential responses to the synthetic opioid fentanyl in male and female mice. We used RNA sequencing and weighted gene co-expression network analysis to show that fentanyl induces discordant transcriptional adaptations in VTA neurons that project to NAc vs PFC. We then used *in vivo* calcium imaging and chemogenetics to determine functional differences in how these projections encode fentanyl-related behavior. We found different timescales of activation between VTA-NAc and VTA-PFC during conditioned place preference that support distinct aspects of fentanyl-context association. Together, our data demonstrate that based on projection target alone, VTA neurons undergo vastly different adaptations in response to fentanyl. This study provides new insight into VTA encoding of opioid behaviors that advance understanding of the neural mechanisms underlying OUD.

INTRODUCTION

Opioid use disorder (OUD) is a chronic, relapsing condition that impacts millions of individuals. The rate of opioid overdose deaths in the U.S. has escalated to unprecedented numbers in recent years, primarily due to increased prevalence of potent synthetic opioids like fentanyl (1). Fentanyl possesses unique pharmacological properties compared to other opioids: its high lipid solubility allows for rapid passage through the blood brain barrier (2), it exhibits unique binding interactions with the mu opioid receptor (3), and distinct receptor selectivity as compared to morphine (4). Fentanyl exposure is associated with poorer treatment outcomes for OUD (5), necessitating novel advances in treatment for OUD cases involving fentanyl. Despite the increased prevalence of fentanyl, an understanding of neuroadaptations resulting from fentanyl misuse remains lacking.

The ventral tegmental area (VTA) is a heterogenous midbrain structure important for opioid reward (6,7) and rodents will self-administer morphine or fentanyl intracranially into this region (8,9). The VTA sends mostly non-overlapping projections to several nodes in the reward circuit, including the nucleus accumbens (NAc) and prefrontal cortex (PFC) (10). While VTA dopamine neurons and their response to drug misuse have been extensively characterized, not all VTA dopamine neurons are functionally identical. Rather, they exhibit several differences depending on their downstream projection target, including baseline electrophysiological differences (10,11), and specific inputs from other regions (12,13). In mouse, VTA dopamine neurons that project to PFC have higher membrane excitability and faster firing rate (10,14–16) and differential expression of dopamine markers (10,17,18) compared to those that project to NAc. VTA dopamine neurons also exhibit projection-specific responses to opioids, including differential degree of recruitment by opioids (19), distinct morphine-induced morphological changes (20), and selective inhibition by kappa opioid agonists (21).

Alongside dopamine, the VTA contains other neuron subtypes capable of releasing glutamate, GABA, or combinations of neurotransmitters (22–24). VTA projections contain different proportions of neurotransmitter subtypes depending on downstream target (25,26). Recent work indicates many behavioral functions classically attributed to VTA dopamine neurons can also be mediated by glutamate (27–30), GABA (31,32), and co-transmitting (33–35) neurons. These functions extend to opioid use, as many VTA neuron subtypes express mu opioid receptors (36), participate in opioid seeking behaviors (37,38), and undergo diverse molecular adaptations following opioid self-administration (23,39). However, it remains unclear whether the projection-specific response

to opioids exhibited by VTA dopamine neurons is shared by other VTA neurons, since most characterizations of VTA circuit function focus on dopamine.

Given the vast heterogeneity in VTA cell types, characterizing VTA function by neurotransmitter identity can be limiting. There is significant overlap among neurotransmitter markers, since the rate limiting enzyme for dopamine synthesis, tyrosine hydroxylase (TH), can be expressed in VTA neurons that release glutamate (40) or GABA (41). Similarly, many VTA neurons that express the vesicular glutamate transporter 2 also express the vesicular GABA transporter and as such release both neurotransmitters (35,42). Oftentimes, VTA neurons expressing the same neurotransmitter markers exhibit opposing activity: VTA dopamine neurons can be activated by both rewarding and aversive stimuli (43), and VTA glutamate neurons can elicit both reward and aversion (33). Further, VTA glutamate and GABA projection neurons form both distal and local connections, suggesting that activity at one cell type is directly influencing activity at other VTA neurons (36). Defining VTA neurons by characteristics other than neurochemical profile, such as their circuit output, can help elucidate VTA encoding of behavior. Since opioids engage neuronal ensembles in the VTA that bypass neurotransmitter type (44,45), this approach may be especially useful in the context of opioid behaviors.

In this study we sought to understand how projection-defined VTA neurons respond to fentanyl and differentially drive drug-context association. We used RNA sequencing to compare fentanyl-induced transcriptional adaptations in VTA neurons that project to either NAc core (VTA-NAc) or medial PFC (VTA-PFC) and identified discordance between projection neuron populations. We then used a combination of *in vivo* approaches to investigate VTA-NAc and VTA-PFC activity during fentanyl conditioned place preference (CPP). Using fiber photometry, we found both projections had increased calcium activity during fentanyl exposure but exhibited temporally distinct calcium dynamics during entries to the fentanyl-paired context. Finally, chemogenetic inhibition of VTA-NAc vs VTA-PFC differentially impacted fentanyl CPP. Together, these studies demonstrate that examining the VTA by its circuit outputs—not just transmitter identity—reveals new ways that its diverse projections shape behavior

MATERIALS AND METHODS

Experimental subjects

All procedures were approved by the Institutional Animal Care and Use Committee at the Pennsylvania State University College of Medicine (PSUCOM) and conducted in accordance with NIH guidelines for the use of laboratory animals. RiboTag mice on a C57BL/6J background were obtained from The Jackson Laboratory (RRID:IMSR_JAX:029977) and bred at PSUCOM. All mice were given food and water *ad libitum* and housed in the PSUCOM vivarium on a 12:12h light:dark cycle with lights on at 7:00. All mice were group housed in corncob bedding and provided with nestlets. After fiber optic implantations, mice were pair-housed across a perforated acrylic divider to prevent isolation stress. All experiments used mice of both sexes aged 8-10 weeks at the start of behavior.

Drugs

Fentanyl citrate (#22659) obtained from Cayman chemical (Ann Arbor, MI), and deschloroclozapine (DCZ) (#7193) obtained from Tocris Bioscience (Minneapolis, MN), were dissolved in sterile saline (0.9%).

Stereotaxic surgery

Adeno-associated viruses for Cre recombinase (AAVrg.hSyn.HI.eGFP-Cre.WPRE.SV40 or AAV9-CMV-PI-Cre), Cre-dependent GCaMP8s (AAV9-syn-FLEX-jGCaMP8s-WPRE), Gi-coupled (AAV9-hSyn-DIO-hM4D(Gi)-mCherry) Designer Receptors Exclusively Activated by Designer Drugs (DREADDs), and mCherry (AAV9-hSyn-DIO-mCherry) were acquired from Addgene (#105540, 105537, 162377, 44362, 50459). AAVs (300nL/side) were delivered intracranially under isoflurane anesthesia as previously described (46), using the following coordinates relative to bregma: NAc core (AP +1.6, ML ±1.5, DV -4.4, 10°), mPFC (AP +1.7, ML ±0.75, DV -2.5, 15°), VTA (AP -3.2, ML ±1.0, DV -4.6, 7°). For fiber photometry, GCaMP was infused unilaterally (AP -3.2, ML +0.4, DV -4.2, 0°), and a 400µm core fiber optic cannula (Thorlabs #CFM14L05) was implanted above the VTA (DV -4.0), and secured to the skull with two screws and C&B Metabond Adhesive Cement (Parkell #S380).

RNA Isolation & Sequencing

Mice were euthanized by cervical dislocation, and brains were rapidly removed and chilled in ice cold PBS. Cold brains were cut into 1 mm coronal sections using an aluminum brain matrix, and tissue punches containing total VTA were collected with 14-gauge needle, then snap-frozen on dry ice and stored at -80 until processing.

Polyribosomes were immunoprecipitated as described previously (47,48), with full details on RNA extraction, library preparation, sequencing, and analysis strategy in **Supplemental Methods.**

Conditioned place preference

Conditioned place preference (CPP) was performed as previously described (46) in a three-chambered rectangular apparatus connected by automatic guillotine doors, and equipped with infrared photobeam detectors that track animal position and movement (ENV-3013, MED Associates). On the first day of testing (pre-test), mice underwent a 5 min habituation in the center compartment, after which the doors opened, and they freely explored the entire apparatus for 20 min. The least-preferred chamber was subsequently assigned as the fentanyl-paired chamber. Mice then underwent 3 consecutive days of conditioning. On conditioning days, mice received an i.p. injection of saline (10 mL/kg) and were confined to the saline-paired compartment for 20 min; 4 h later, they received an i.p. injection of fentanyl (0.2 mg/kg) and were confined to the fentanyl-paired compartment for 20 min. On the fifth day of testing (post-test), after 5 min habituation in the center, they freely explored the entire apparatus for 20 min. Locomotion was measured as movement counts in Med-PC V Software.

Fiber photometry

Three weeks after surgery, mice were habituated to a dummy headstage in their homecage (2-3 days, ~10 min/day). Changes in GCaMP8s fluorescence were acquired with a TeleFipho Wireless Fiber Photometry system (Amuza, San Diego, California) and synchronized to behavioral events with TTL pulses via an AD instruments Interface and Lab Chart Lightning software. Prior to the first behavioral test, a >10 minute recording was taken to confirm GCaMP expression. A >5 minute recording was taken immediately prior to each CPP session to minimize signal decay during testing. Recordings were taken for pre-test, post-test, and all conditioning sessions (470 nm LED @ ~30uW excitation power; 500-550 nm emission). After testing completed, mice were perfused and brains processed for immunostaining as described below to confirm viral expression and fiber placement.

Chemogenetics

At least 14 days after stereotaxic surgery, mice underwent fentanyl CPP as described above. On the fifth day, mice received i.p. injection of saline (or DCZ) 20 min before the post-test. Four hours later, mice were injected with 0.1 mg/kg DCZ (or saline) 20 min before a second post-test (46). After testing, mice were euthanized and a stereomicroscope equipped with a fluorescence adapter (NightSea, Hatfield PA) was used to confirm GFP- Cre expression in projection targets and hM4Gi-mCherry expression in VTA.

Immunostaining and cell counting

Mice were transcardially perfused with PBS and 4% paraformaldehyde. Brains were removed and post-fixed for 24hr, then 50 µm sections collected with a compresstome (Precisionary Instruments, Ashland MA.). Sections containing VTA and projection target were immunostained as previously described (46), using the following primary (1:1000) and secondary (1:500) antibodies: (chicken anti-GFP, Aves Lab, Tigard, OR, #GFP-1020; rabbit anti-TH, Calbiochem #657012; Goat anti-Chicken-FITC, Aves Lab, #F-1005; Donkey anti-Rabbit Alexa Fluor 594, Jackson Immuno, West Grove, PA, #711-585-152). Sections were counterstained with DAPI, mounted with Fluoromount-G (Southern Biotech, Birmingham, AL), and imaged on imaged on a confocal (Leica SP8) or epifluorescence microscope (Nikon Labophot2) to confirm viral expression. Full details are in **Supplemental Methods**. A subset of mice received stereotaxic surgery to express GCaMP as above, but did not receive a fiber optic cannula to avoid tissue damage artifacts. Three VTA images per mouse were acquired with a confocal (Leica SP8), then two investigators independently counted the number of GCaMP and TH expressing neurons in VTA. Percentages obtained by each investigator were averaged together to obtain one value per image.

Data analysis

Full descriptions of differential expression, WGCNA, and fiber photometry calcium imaging analyses are in **Supplemental Methods**. Most data were analyzed with GraphPad Prism 10, and were collapsed across sex in the absence of significant sex effects. For calcium activity during drug exposure, we only included mice with all 6 conditioning recordings, and data were analyzed with paired t-tests. For calcium activity during CPP test days, only the first 15 transitions into each region were analyzed for each mouse to control for behavioral differences (minimum number of transitions observed across all mice), and were analyzed with bootstrapped 95% confidence intervals in MATLAB (49). For chemogenetic experiments, data were analyzed with two-way repeated measures ANOVA with factors of virus and agonist, and significant interactions were followed up with Sidak's post hoc. Mice that did not develop a preference for the fentanyl-paired context were excluded from analysis (n=2).

RESULTS

Discordant fentanyl-induced transcriptional adaptations in VTA-NAc and VTA-PFC

Mesocortical and mesolimbic VTA neurons exhibit diverse morphologic adaptations and differential immediate early gene induction following chronic opioid exposure (19,20). To examine if similar projection-specific adaptations occur at the transcriptional level, we used a retrograde Cre virus in either NAc core or PFC in Ribotag mice to tag ribosomes in specific VTA projection neurons (**Fig 1A**). Mice received one week of fentanyl injections, using a dose that produces physical dependence and locomotor sensitization (50). After 24h abstinence, we isolated and sequenced ribosome-associated RNA from VTA neurons projecting to either NAc or PFC, along with RNA from the input fraction representing total VTA. First, to confirm projection neuron enrichment, we compared expression of several cell-type markers in the immunoprecipitated samples relative to input in saline-treated mice. We found significant enrichment of general neuronal markers (*Mapt*, *Tubb3*, *Map2*, *Nlgn3*, *Nefl, Eno2,* p's≤ 4.2×10^{-5}), and de-enrichment of markers for oligodendrotyces (*Aspa*), astrocytes (*Slc1a3*), microglia (*Arhgap15*), and pericytes (*Pla1a*, p's≤ 6.4×10^{-5}; **Fig 1B**). We next looked for enrichment of neuron subtype markers, and identified heterogeneity in both samples (**Fig 1B**): In VTA-PFC, we found significant enrichment of several monoaminergic, glutamatergic, and GABAergic markers; in VTA-NAc, we found enrichment of monoaminergic and glutamatergic markers, alongside *Crhbp*, which is enriched in co-transmitter populations (22,23,51). In the VTA-NAc samples we also found enrichment of *Crhr1* and de-enrichment of *Cck* (0.47 vs -0.35 fold change, respectively), demonstrating our VTA-NAc population are primarily core-projecting (52).

We next examined the top differentially expressed protein coding genes in the mesocortical vs mesolimbic populations following fentanyl exposure and compared them with the top differentially expressed genes (DEGs) in total VTA (**Fig 1C,** all genes in **Supplemental File 1**). Strikingly, there was little concordance in the top 5 most up- and downregulated genes, with some genes showing opposite expression changes in the projection-specific populations (e.g. *Gbx2* and *Lhx9* downregulated in VTA-PFC and upregulated in VTA-NAc). The only statistically significant concordant gene was *Chrna2*, which demonstrated a similar degree of upregulation across the three populations. There was little overlap when extending the comparison to any DEG with $p<0.05$, with most showing expression changes in only one population (**Fig 1D**). Further, nearly twice as many genes were differentially expressed in VTA-PFC vs VTA-NAc (VTA-PFC: 1100 upregulated, 1071 downregulated; VTA-NAc: 379 upregulated, 592 downregulated; **Supplemental File 1**). To ensure the observed discordance was not driven by arbitrary p-value cutoffs, we next applied rank-rank hypergeometric overlap

(RRHO) analysis. This threshold-free method assesses the significance of overlap between two gene lists ranked by their degree of differential expression rather than by p-value (53,54). We first compared fentanyl-induced gene expression changes in input to either VTA-PFC or VTA-NAc and expected significant overlap as these populations are part of total VTA. For both comparisons we found significant overlap in the upper right and lower left quadrants, indicating concordance (**Fig 1E-G**), although the overlap between total VTA and VTA-PFC was greater relative to VTA-NAc. When comparing ranked gene lists between VTA-PFC and VTA-NAc, we found significant overlap in the upper left and lower right quadrants, revealing significant discordance (**Fig 1H**), confirming fentanyl dysregulated genes diverge between projection populations regardless of p-value cutoffs.

To further characterize transcriptional adaptations in the mesocortical and mesolimbic neurons, we next performed weighted gene co-expression network analysis (WGCNA) separately in each projection neuron population. We identified 28 modules of co-expressed genes in VTA-PFC, and 14 in VTA-NAc with a $p<0.05$ effect of fentanyl in either sex, or with sexes combined (**Fig 1I-J, Supplemental File 1**). To define the functional enrichment within the fentanyl associated modules, we performed gene ontology (GO) analysis on the genes within each module (Top terms in **Fig 2A,C**, all enrichments in **Supplemental File 1**). Genes in upregulated VTA-PFC modules were enriched for neurotransmission-related terms, such as neurotransmitter reuptake (P23), positive regulation of dopamine secretion (P64), and G protein activity (P66). Genes in downregulated VTA-PFC modules also reflected neurotransmission, such as synaptic vesicle (P4), regulation of postsynaptic membrane potential (P17), and regulation of cytosolic calcium (P39; **Fig 2A**). Genes in upregulated VTA-NAc modules were enriched for several metabolic terms such as N-acylethanolamine metabolism (N39) and regulation of reactive oxygen species metabolism (N29), while genes in downregulated VTA-NAc modules were enriched for terms like translation initiation (N28) and protein targeting to endoplasmic reticulum (N18; **Fig 2C**). We then visualized four gene networks per population, based on the top upregulated and downregulated eigengenes, along with an upregulated and downregulated module enriched for GO terms of interest (**Fig 2B,D**). We identified several hub genes of interest in our selected modules: For VTA-PFC, these include upregulated phosphoinositide 3-kinase *Pik3c2b* (P43), vesicular monoamine transporter *Slc18a2* (P23), and downregulated L-type calcium channel subunit *Cacnb1* (P16) and calcium-binding *Calb2* (Calretinin; P4; **Fig 2B**). For VTA-NAc, these include upregulated acetylcholine receptor regulator *Lypd6b* (N39), upregulated transcription factors *Mef2c* and *Foxg1* (N29), and downregulated chromatin regulators *Mrbgp* (N21) and *Rbm14* (N18; **Fig 2D**).

Given the overrepresentation of transcription factors in VTA-NAc, we looked for additional transcriptional regulators of our select gene networks with iRegulon (55) (top transcription factors for select modules in **Fig 2E,G,** all in **Supplemental File 1**). Informed by prior literature, we chose a transcription factor from each projection group previously implicated in substance use disorders for visualization (56,57). For VTA-PFC, we chose *Creb1*, which was the top regulator for P43 (**Fig 2F**). While *Creb1* itself was not changed, 19 of its target genes were upregulated as a function of fentanyl. For VTA-NAc, we found *Mef2c*, a N29 hub gene, was also the top regulator of N29 (**Fig 2H**).

Both VTA-NAc and VTA-PFC exhibit elevated calcium activity during fentanyl conditioning

Given the distinct fentanyl-induced transcriptional adaptations occurring in VTA-NAc and VTA-PFC, we next asked whether they exhibited different fentanyl-associated activity. We used fiber photometry to measure calcium activity of VTA-NAc and VTA-PFC during fentanyl conditioned place preference (CPP ;**Fig 3A**). Like our RNA sequencing, we found heterogeneity in VTA projections expressing GCaMP, with 32.5% of VTA-NAc and 28.4% of VTA-PFC GCaMP neurons colocalizing with TH (**Fig 3B**; n=5 mice per projection target group, 3 images per mouse; VTA-NAc vs VTA-PFC t-test, t_8=1.22, p=0.26). All mice spent more time in the fentanyl-paired context during the post-test vs pre-test (**Fig 3C**; session $F_{1,18}$=63.19, p<0.0001; projection target group $F_{1,18}$=0.30, p=0.59). To examine VTA projection activity during fentanyl exposure we analyzed photometry data from conditioning sessions (**Fig 3D**). With no main effects of conditioning day, data were averaged across days and analyzed with paired t-test. For both VTA-NAc and VTA-PFC neurons, we found more calcium transients during fentanyl conditioning relative to saline (VTA-NAc: **Fig 3E**, t_8=3.79, p=0.005; VTA-PFC: **Fig 3F**, t_5=4.04, p=0.0099). There were no differences in average transient amplitude (VTA-NAc: t_8=0.68, p=0.52; VTA-PFC: t_5=1.45, p=0.21). We then analyzed transient frequency during the post-test and found signals resembling reward prediction error. VTA-NAc had reduced transient frequency when mice were in the fentanyl-paired vs saline-paired context (**Fig 3G**, t_9=2.32, p=0.046) and VTA-PFC had a similar, but not significant trend (**Fig 3H**, t_9=1.84, p=0.099). There were no differences in average transient amplitude in the saline- vs fentanyl-paired context (VTA-NAc: t_9=0.93, p=0.38; VTA-PFC: t_9=0.006, p=0.995).

Distinct calcium dynamics of VTA-NAc and VTA-PFC during entries to the fentanyl-paired context

Next, we asked if VTA-NAc and VTA-PFC were differentially engaged during entry into the fentanyl-paired context, as others have shown VTA calcium increases during entry to a cocaine-paired context (58). Using

bootstrapped 95% confidence intervals (49), we identified greater calcium activity in VTA-NAc in the one second preceding entries to the fentanyl-paired context relative to saline (**Fig 4A,G**). In contrast, VTA-PFC peaked earlier at ~2 seconds prior to fentanyl-paired entry (**Fig 4C,H**). The increased calcium activity in VTA projections during fentanyl-paired entries did not reflect exits from the saline-paired context, since there were no differences in activity when aligned to region exits (**Fig 4A,C**). We did not identify any signals consistent with extinction, as the increased activity preceding fentanyl-paired entry was consistent throughout the session for both projections (**Fig 4B,D**). To ensure these effects were consistent across mice, we calculated each mouse's mean zΔF/F in 1 second bins preceding region entries (-2s to -1s from entry, and -1s to 0s from entry) and used paired t-tests to compare saline- and fentanyl-paired entries. During the pre-test, there were no differences in the binned mean zΔF/F preceding region entries for both VTA-NAc (**Fig 4E**) and VTA-PFC (**Fig 4F**). For post-test, like we observed with bootstrapped confidence intervals, VTA-NAc mean zΔF/F was greater in the -1s to 0s from fentanyl-paired vs saline-paired entries after conditioning (**Fig 4G**, t_9=2.39, p=0.041). For VTA-PFC, there was a trend towards greater mean zΔF/F during fentanyl-paired entries at both -2s to -1s (**Fig 4H**, left; t_9=2.23, p=0.052) and -1s to 0s (**Fig 4H**, right; t_9=1.98, p=0.079).

Chemogenetic inhibition of VTA-NAc vs VTA-PFC impact distinct processes in fentanyl conditioned place preference

Finally, we used chemogenetics to determine whether the different activity of VTA-NAc vs VTA-PFC observed with fiber photometry promotes different behavioral outcomes in fentanyl CPP. We expressed the inhibitory DREADD hM4Di, or an mCherry control, in either VTA-NAc or VTA-PFC. Using a counterbalanced, within-subject design, mice underwent two post-tests 4 hours apart, each preceded by an injection of the DREADDs agonist DCZ or vehicle (**Fig 5A**). Inhibiting VTA-NAc reduced time spent in the fentanyl-paired context (**Fig 5B**, virus x agonist $F_{1,21}$=5.04, p=0.036; Sidak's post hoc, vehicle vs DCZ: hM4Gi p=0.012, mCherry p=0.95). This was not due to differences in entries into the fentanyl-paired (**Fig 5C**, virus x agonist $F_{1,21}$=2.39, p=0.14) or saline-paired contexts (**Fig 5D**, virus x agonist $F_{1,21}$=2.02. p=0.17), nor reduced locomotion (**Fig 5E**, virus x agonist $F_{1,21}$=2.74, p=0.11). In contrast, inhibiting VTA-PFC did not alter time spent in the fentanyl-paired context (**Fig 5F**, virus x agonist $F_{1,20}$=3.17, p=0.093; Sidak's post hoc, vehicle vs DCZ: mCherry p=0.36, hM4Gi p=0.44). However, this did reduce entries to the fentanyl-paired context (**Fig 5G**, virus x agonist $F_{1,20}$=4.45, p=0.048; Sidak's post hoc, vehicle vs DCZ: mCherry p=0.84, hM4Gi p=0.046) but not the saline-paired context (**Fig 5H**,

virus x agonist $F_{1,20}$=3.55, p=0.074; Sidak's post hoc, vehicle vs DCZ: mCherry p=0.70, hM4Gi p=0.14). Inhibition of VTA-PFC also reduced total movement counts (**Fig 5I**, virus x treatment $F_{1,20}$=7.42, p=0.013 Sidak's post hoc, vehicle vs DCZ: mCherry p=0.45, hM4Gi p=0.028).

DISCUSSION

In this study we demonstrated that fentanyl induces distinct molecular and functional adaptations in VTA neurons depending on their downstream projection target. We used RNA sequencing to show that chronic fentanyl induces remarkably discordant translatomes in VTA neurons that project to NAc vs PFC. We then demonstrated these differences are functionally reflected in projection-specific encoding of fentanyl-associated behavior. We found VTA-NAc and VTA-PFC exhibit distinct signals during fentanyl-context associations, and that inhibiting either projection impacts different processes in the behavior. These experiments provide unique insight into the molecular and activity profiles of specific VTA projections in response to fentanyl, revealing new ways that VTA circuits shape opioid-associated behaviors.

Projection-specific VTA neurons undergo discordant fentanyl-induced molecular changes

To investigate fentanyl-induced molecular adaptations in VTA projections, we sequenced ribosome-associated RNA from VTA-NAc and VTA-PFC neurons after chronic fentanyl exposure and found robust discordance in differential gene expression between the projections. Even the most upregulated and most downregulated genes differed between the projections . While this revealed some DEGs with novel links to opioids (e.g. *Npvf*, *Gbx2*, *Prg4*), we also revealed several DEGs with prior implications for other misused drugs. Some examples include *Ttr* and *Slc13a4*, which are upregulated in input and VTA-PFC in our dataset and in other brain regions after cocaine exposure (59–61), and *Tcf19,* which is downregulated in VTA-PFC and VTA-NAc in our dataset and in PFC after chronic cocaine (62). Since these genes are implicated across brain regions and with multiple substances, they make promising targets for future substance use research.

A notable difference between VTA projections includes the function of genes impacted by fentanyl. The VTA-PFC gene ontology largely reflect changes to neuronal plasticity and excitability. Similar opioid-induced adaptations occur in VTA dopamine neurons (7), but the extent to which these adaptations are projection-dependent is unclear. Terms like "collagen fibril organization," "extracellular matrix," and "actin binding" appear across several upregulated VTA-PFC modules, reflecting upregulated structural plasticity. This is reminiscent of

chronic morphine increasing soma size exclusively in VTA-PFC dopamine neurons (20) and increasing dendrite diameter of dopamine neurons in the parabrachial VTA, where PFC-projecting neurons primarily reside (63). Several synaptic GO terms (synaptic vesicle, presynaptic active zone, presynaptic cytosol, axonogenesis, neuron projection terminus) across downregulated VTA-PFC modules indicate altered synaptic plasticity in this projection. We also found “positive regulation of cytosolic calcium ion concentration” representing P39, alongside downregulation of the voltage-gated calcium channel *Cancb1* and the intracellular calcium regulator *Calb2*, reflecting altered excitability. While these adaptations were less apparent in VTA-NAc, we did find several GO terms and DEGs with implications for opioid behaviors. A notable GO term is “regulation of reactive oxygen species (ROS) metabolic processes,” representing N29. Opioids induce ROS-dependent DNA damage in PFC and NAc that potentiate heroin seeking behavior (64), but such a mechanism has not been explored in VTA. Another notable GO term is “NAE metabolic process,” representing N39. This refers to a key component of endocannabinoid signaling, which has a role in natural reward signaling through VTA-NAc (65) that may extend to opioid reward. *Naaa* is a notable upregulated gene in this GO term and a promising molecular target, as intra-VTA NAAA inhibition reduces alcohol motivation in rats (66). Discordant transcriptional adaptations across projections likely contribute to projection-specific roles in opioid-related behavior, but additional work is needed to test the causal role of individual genes in each projection.

We chose select gene modules for further visualization of the gene network and identification of transcriptional regulators, highlighting several potential gene targets and their associated transcription factors. A notable upregulated hub gene is *Lypd6b* (N39), which encodes a modulator of nicotinic acetylcholine receptors. Nicotinic acetylcholine receptors are significant as they are expressed on all VTA neuron subtypes (67), are necessary for morphine CPP (68), and *Chrna2*, encoding the nicotinic alpha2 subunit, is one of the few upregulated genes shared across all VTA populations. Cholinergic inputs to VTA may serve to further functionally distinguish VTA projections, as mesolimbic dopamine neurons are selectively excited by specific cholinergic inputs (69). Another notable upregulated hub gene is *Mef2c* (N29), which also transcriptionally regulates other N29 genes. *Mef2c*, encoding myocyte enhancer factor 2C, has been implicated as an addiction-relevant transcription factor (56,57), mainly for its role in regulating structural plasticity in the NAc that promotes cocaine behavior (70,71), but a connection to opioid actions in VTA has not been previously identified. In VTA-PFC we found *Creb1*, encoding the cAMP responsive element binding protein that has been implicated in cocaine (72,73),

nicotine (74), alcohol (75), and morphine misuse (76–78). While there has been much focus on CREB function in NAc and locus coeruleus (56,57), its role in VTA warrants further investigation.

Projection-specific VTA neurons encode functionally distinct processes in fentanyl CPP

Given the extensive discordance in fentanyl-induced transcriptional adaptations between VTA projections, we sought to understand whether this extends to different functions in fentanyl-associated behavior. We chose a fentanyl CPP paradigm because it is multifaceted (direct fentanyl exposure and fentanyl-context associations), robust (>95% of mice developed a preference for the fentanyl-paired context), and allows for within-subject comparisons (fentanyl vs saline, repeated preference testing). VTA activity is essential for CPP, since VTA activity increases during entries to a cocaine-paired context (58) and VTA inactivation inhibits cocaine CPP (79). While prior work has characterized dopamine actions in CPP (79–81), dopamine is not necessarily essential for CPP, since dopamine deficient mice form place preferences for cocaine and morphine (82,83). Therefore, a new approach to investigating VTA function in CPP improves our understanding of how drug-context associations are formed.

Here we found VTA-NAc and VTA-PFC increased activity during fentanyl exposure, consistent with classic opioid-mediated disinhibition in the VTA. After conditioning, VTA-PFC activity increased earlier in the transition to the fentanyl-paired context, potentially reflecting a decision-making process. In contrast, VTA-NAc activity peaked later in the transition, likely a response to drug-associated contextual cues, and exhibited decreased transient frequency when mice were in the fentanyl-paired context, reminiscent of a reward prediction error signal. Although both projections signaled the place preference, they likely reflect separate processes, because chemogenetic inhibition of each projection produced different behavioral outcomes. Inhibiting VTA-NAc reduced time spent in the fentanyl-paired context, suggesting this projection encodes the value of the fentanyl-paired context. Meanwhile, inhibiting VTA-PFC reduced entries to the fentanyl-paired context, suggesting this projection supports the decision to go to the fentanyl-paired context. Importantly, reduced entries to the fentanyl-paired context are not an artifact of reduced locomotion, because entries to the saline-paired context were unaffected. Rather, it is possible that reduced locomotion reflects increased decision-making time.

An important consideration is the heterogeneity in neurotransmitter profiles of the VTA projections represented in this study. Our cell-type characterizations reveal we serendipitously overrepresented the non-dopaminergic proportion of VTA projections. Our immunolabelling revealed ~30% of GCaMP-expressing neurons

were TH-positive in both projections. The proportion of TH+ VTA projection neurons varies with the method used. For example, retrograde tracers like Fluorogold reveal ~70% of mouse VTA projection neurons are TH+ (25), while Cre-expressing canine adenoviruses show more TH+ VTA-NAc (60%) than VTA-PFC (40%) (12). Unexpectedly, in our RNA sequencing experiments, we found VTA-NAc had lower enrichment of several dopaminergic markers compared to VTA-PFC. We suspect this reflects differences in AAV transduction efficiency and not a true difference in the proportion of dopaminergic cell types between the projections. Indeed, others have shown that midbrain dopamine neurons are not efficiently captured by most AAV serotypes (84), and while different baseline properties of dopaminergic neurons across projections may influence their intrinsic tropism for AAVs, this requires further investigation. Despite a limited number of TH-expressing neurons, our experiments support functions often attributed to dopamine neurons can also be mediated by other VTA neurons.

Conclusions

Here we demonstrate distinct properties of projection-defined VTA neurons across multiple fentanyl modalities. Depending on their downstream projection target, VTA neurons adopt different fentanyl-induced translatome profiles and fentanyl-associated activity profiles. We identified several promising candidate genes and transcription factors, some novel and some with prior brain-wide implications for substance use disorders. We also elucidated how projection-specific VTA populations encode fentanyl-context associations independent of neurotransmitter identity, providing a previously under-appreciated viewpoint of VTA representations of opioid behaviors. These findings provide necessary insight to the circuit-level neuroadaptations resulting from fentanyl, thus improving our understanding of potential neural mechanisms underlying OUD.

Acknowledgements

The authors thank the Penn State College of Medicine Genome Sciences Core (RRID:SCR_021123) and Advanced Light Microscopy Core (RRID:SCR_022526). A version of this manuscript was previously uploaded to bioRxiv as a preprint (https://doi.org/10.1101/2025.11.26.690827).

Conflicts of Interest: The authors have no competing interests to declare.

Author Contributions

AM and MEF designed the experiments. AM, HS, LDF, LBM, AEO, and SP performed behavior experiments. MEF performed RNA isolation. AM and KD counted cells. AM, HS, and MEF performed data analysis. AM and MEF wrote the manuscript and prepared the figures with input from all authors.

Funding

This work was supported by NIH grant DP1 DA058661 awarded to MEF.

Data and code availability

RNAseq data have been deposited at GEO and are publicly available as of the date of publication (GSE313440). Differential expression, WGCNA, and all code are available at github.com/mfoxlab.

References

1. Spencer MR, Garnett MF, Miniño AM. Drug Overdose Deaths in the United States, 2002–2022. NCHS Data Brief, no 491 [Internet]. 2024;Hyattsville, MD: National Center for Health Statistics. Available from: https://dx.doi.org/10.15620/cdc:135849

2. Kelly E, Sutcliffe K, Cavallo D, Ramos-Gonzalez N, Alhosan N, Henderson G. The anomalous pharmacology of fentanyl. British J Pharmacology. 2023 Apr;180(7):797–812.

3. Sutcliffe KJ, Corey RA, Alhosan N, Cavallo D, Groom S, Santiago M, et al. Interaction With the Lipid Membrane Influences Fentanyl Pharmacology. Adv Drug Alcohol Res. 2022 Mar 21;2:10280.

4. Eshleman AJ, Nagarajan S, Wolfrum KM, Reed JF, Nilsen A, Torralva R, et al. Affinity, potency, efficacy, selectivity, and molecular modeling of substituted fentanyls at opioid receptors. Biochemical Pharmacology. 2020 Dec;182:114293.

5. Socias ME, Wood E, Le Foll B, Lim R, Choi JC, Mok WY, et al. Impact of fentanyl use on initiation and discontinuation of methadone and buprenorphine/naloxone among people with prescription-type opioid use disorder: secondary analysis of a Canadian treatment trial. Addiction. 2022 Oct;117(10):2662–72.

6. Koob GF, Volkow ND. Neurocircuitry of Addiction. Neuropsychopharmacol. 2010 Jan;35(1):217–38.

7. Doyle MA, Mazei-Robison MS. Opioid-Induced Molecular and Cellular Plasticity of Ventral Tegmental Area Dopamine Neurons. Cold Spring Harb Perspect Med. 2021 Feb;11(2):a039362.

8. Bozarth MA, Wise RA. Intracranial self-administration of morphine into the ventral tegmental area in rats. Life Sciences. 1981 Feb;28(5):551–5.

9. Van Ree JM, De Wied D. Involvement of neurohypophyseal peptides in drug-mediated adaptive responses. Pharmacology Biochemistry and Behavior. 1980 Jan;13:257–63.

10. Lammel S, Hetzel A, Häckel O, Jones I, Liss B, Roeper J. Unique Properties of Mesoprefrontal Neurons within a Dual Mesocorticolimbic Dopamine System. Neuron. 2008 Mar;57(5):760–73.

11. Margolis EB, Mitchell JM, Ishikawa J, Hjelmstad GO, Fields HL. Midbrain Dopamine Neurons: Projection Target Determines Action Potential Duration and Dopamine D_2 Receptor Inhibition. J Neurosci. 2008 Sep 3;28(36):8908–13.

12. Beier KT, Steinberg EE, DeLoach KE, Xie S, Miyamichi K, Schwarz L, et al. Circuit Architecture of VTA Dopamine Neurons Revealed by Systematic Input-Output Mapping. Cell. 2015 Jul;162(3):622–34.

13. Elum JE, Szelenyi ER, Juarez B, Murry AD, Loginov G, Zamorano CA, et al. Distinct dynamics and intrinsic properties in ventral tegmental area populations mediate reward association and motivation. Cell Reports. 2024 Sep;43(9):114668.

14. Chaudhury D, Walsh JJ, Friedman AK, Juarez B, Ku SM, Koo JW, et al. Rapid regulation of depression-related behaviours by control of midbrain dopamine neurons. Nature. 2013 Jan;493(7433):532–6.

15. Friedman AK, Walsh JJ, Juarez B, Ku SM, Chaudhury D, Wang J, et al. Enhancing Depression Mechanisms in Midbrain Dopamine Neurons Achieves Homeostatic Resilience. Science. 2014 Apr 18;344(6181):313–9.

16. Juarez B, Han MH. Diversity of Dopaminergic Neural Circuits in Response to Drug Exposure. Neuropsychopharmacol. 2016 Sep;41(10):2424–46.

17. Lewis DA, Melchitzky DS, Sesack SR, Whitehead RE, Sungyoung Auh, Sampson A. Dopamine transporter immunoreactivity in monkey cerebral cortex: Regional, laminar, and ultrastructural localization. J of Comparative Neurology. 2001 Mar 26;432(1):119–36.

18. Sesack SR, Hawrylak VA, Matus C, Guido MA, Levey AI. Dopamine Axon Varicosities in the Prelimbic Division of the Rat Prefrontal Cortex Exhibit Sparse Immunoreactivity for the Dopamine Transporter. J Neurosci. 1998 Apr 1;18(7):2697–708.

19. Morison SL, Doster LB, Vigotsky AD, Centeno MV, Lopez Gonzalez Del Rey N, Apkarian AV, et al. Recruitment of specific dopamine neuron sub-circuits by opioids. Addiction Neuroscience. 2025 Dec;17:100233.

20. Simmons SC, Wheeler K, Mazei-Robison MS. Determination of circuit-specific morphological adaptations in ventral tegmental area dopamine neurons by chronic morphine. Mol Brain. 2019 Dec;12(1):10.

21. Margolis EB, Lock H, Chefer VI, Shippenberg TS, Hjelmstad GO, Fields HL. κ opioids selectively control dopaminergic neurons projecting to the prefrontal cortex. Proc Natl Acad Sci USA. 2006 Feb 21;103(8):2938–42.

22. Phillips RA, Tuscher JJ, Black SL, Andraka E, Fitzgerald ND, Ianov L, et al. An atlas of transcriptionally defined cell populations in the rat ventral tegmental area. Cell Reports. 2022 Apr;39(1):110616.

23. Fox ME, Montemarano A, Ostman AE, Basu M, Herb B, Ament SA, et al. Transcriptional signatures of fentanyl use in the mouse ventral tegmental area. Addiction Biology. 2024 May;29(5):e13403.

24. Fitzgerald ND, Day JJ. Neuronal heterogeneity in the ventral tegmental area: Distinct contributions to reward circuitry and motivated behavior. Addiction Neuroscience. 2025 Mar;14:100191.

25. Taylor SR, Badurek S, Dileone RJ, Nashmi R, Minichiello L, Picciotto MR. GABAergic and glutamatergic efferents of the mouse ventral tegmental area. J of Comparative Neurology. 2014 Oct;522(14):3308–34.

26. Breton JM, Charbit AR, Snyder BJ, Fong PTK, Dias EV, Himmels P, et al. Relative contributions and mapping of ventral tegmental area dopamine and GABA neurons by projection target in the rat. J of Comparative Neurology. 2019 Apr;527(5):916–41.

27. Root DH, Mejias-Aponte CA, Qi J, Morales M. Role of Glutamatergic Projections from Ventral Tegmental Area to Lateral Habenula in Aversive Conditioning. J Neurosci. 2014 Oct 15;34(42):13906–10.

28. Wang HL, Qi J, Zhang S, Wang H, Morales M. Rewarding Effects of Optical Stimulation of Ventral Tegmental Area Glutamatergic Neurons. J Neurosci. 2015 Dec 2;35(48):15948–54.

29. McGovern DJ, Polter AM, Root DH. Neurochemical Signaling of Reward and Aversion to Ventral Tegmental Area Glutamate Neurons. J Neurosci. 2021 Jun 23;41(25):5471–86.

30. Zell V, Steinkellner T, Hollon NG, Warlow SM, Souter E, Faget L, et al. VTA Glutamate Neuron Activity Drives Positive Reinforcement Absent Dopamine Co-release. Neuron. 2020 Sep;107(5):864-873.e4.

31. van Zessen R, Phillips JL, Budygin EA, Stuber GD. Activation of VTA GABA Neurons Disrupts Reward Consumption. Neuron. 2012 Mar;73(6):1184–94.

32. Tan KR, Yvon C, Turiault M, Mirzabekov JJ, Doehner J, Labouèbe G, et al. GABA Neurons of the VTA Drive Conditioned Place Aversion. Neuron. 2012 Mar;73(6):1173–83.

33. Warlow SM, Singhal SM, Hollon NG, Faget L, Dowlat DS, Zell V, et al. Mesoaccumbal glutamate neurons drive reward via glutamate release but aversion via dopamine co-release. Neuron. 2024 Feb;112(3):488-499.e5.

34. Root DH, Barker DJ, Estrin DJ, Miranda-Barrientos JA, Liu B, Zhang S, et al. Distinct Signaling by Ventral Tegmental Area Glutamate, GABA, and Combinatorial Glutamate-GABA Neurons in Motivated Behavior. Cell Reports. 2020 Sep;32(9):108094.

35. Yoo JH, Zell V, Gutierrez-Reed N, Wu J, Ressler R, Shenasa MA, et al. Ventral tegmental area glutamate neurons co-release GABA and promote positive reinforcement. Nat Commun. 2016 Dec 15;7(1):13697.

36. Oriol L, Chao M, Kollman GJ, Dowlat DS, Singhal SM, Steinkellner T, et al. Ventral tegmental area interneurons revisited: GABA and glutamate projection neurons make local synapses. eLife. 2025 Apr 16;13:RP100085.

37. Bossert JM, Liu SY, Lu L, Shaham Y. A Role of Ventral Tegmental Area Glutamate in Contextual Cue-Induced Relapse to Heroin Seeking. J Neurosci. 2004 Nov 24;24(47):10726–30.

38. McGovern DJ, Polter AM, Prévost ED, Ly A, McNulty CJ, Rubinstein B, et al. Ventral tegmental area glutamate neurons establish a mu-opioid receptor gated circuit to mesolimbic dopamine neurons and regulate opioid-seeking behavior. Neuropsychopharmacol. 2023 Dec;48(13):1889–900.

39. Browne CJ, Futamura R, Minier-Toribio A, Hicks EM, Ramakrishnan A, Martínez-Rivera FJ, et al. Transcriptional signatures of heroin intake and relapse throughout the brain reward circuitry in male mice. Sci Adv. 2023 Jun 9;9(23):eadg8558.

40. Stuber GD, Hnasko TS, Britt JP, Edwards RH, Bonci A. Dopaminergic Terminals in the Nucleus Accumbens But Not the Dorsal Striatum Corelease Glutamate. Journal of Neuroscience. 2010 Jun 16;30(24):8229–33.

41. Lammel S, Steinberg EE, Földy C, Wall NR, Beier K, Luo L, et al. Diversity of Transgenic Mouse Models for Selective Targeting of Midbrain Dopamine Neurons. Neuron. 2015 Jan;85(2):429–38.

42. Root DH, Mejias-Aponte CA, Zhang S, Wang HL, Hoffman AF, Lupica CR, et al. Single rodent mesohabenular axons release glutamate and GABA. Nat Neurosci. 2014 Nov;17(11):1543–51.

43. Holly EN, Miczek KA. Ventral tegmental area dopamine revisited: effects of acute and repeated stress. Psychopharmacology. 2016 Jan;233(2):163–86.

44. Wang F, Liu C bao, Wang Y, Wang X xi, Yang Y yao, Jiang C you, et al. Morphine- and foot shock-responsive neuronal ensembles in the VTA possess different connectivity and biased GPCR signaling pathway. Theranostics. 2024;14(3):1126–46.

45. Koutlas I, Patrikiou L, Van Der Starre SE, Danko D, Wolterink-Donselaar IG, Luijendijk MCM, et al. Distinct ventral tegmental area neuronal ensembles are indispensable for reward-driven approach and stress-driven avoidance behaviors [Internet]. 2024 [cited 2025 Nov 25]. Available from: http://biorxiv.org/lookup/doi/10.1101/2024.05.30.596611

46. Montemarano A, Fox LD, Alkhaleel FA, Ostman AE, Sohail H, Pandey S, et al. A Drd1-cre mouse line with nucleus accumbens gene dysregulation exhibits blunted fentanyl seeking. Neuropsychopharmacology. 2025 Feb 19;50:1993–2005.

47. Fox ME, Chandra R, Menken MS, Larkin EJ, Nam H, Engeln M, et al. Dendritic remodeling of D1 neurons by RhoA/Rho-kinase mediates depression-like behavior. Mol Psychiatry. 2020 May;25(5):1022–34.

48. Fox ME, Wulff AB, Franco D, Choi EY, Calarco CA, Engeln M, et al. Adaptations in Nucleus Accumbens Neuron Subtypes Mediate Negative Affective Behaviors in Fentanyl Abstinence. Biological Psychiatry. 2023 Mar;93(6):489–501.

49. Jean-Richard-dit-Bressel P, Clifford CWG, McNally GP. Analyzing Event-Related Transients: Confidence Intervals, Permutation Tests, and Consecutive Thresholds. Front Mol Neurosci. 2020 Feb 6;13:14.

50. Uddin O, Jenne C, Fox ME, Arakawa K, Keller A, Cramer N. Divergent profiles of fentanyl withdrawal and associated pain in mice and rats. Pharmacology Biochemistry and Behavior. 2021 Jan;200:173077.

51. Simon RC, Loveless MC, Yee JX, Goh B, Cho SG, Nasir Z, et al. Opto-seq reveals input-specific immediate-early gene induction in ventral tegmental area cell types. Neuron. 2024 Aug;112(16):2721-2731.e5.

52. Heymann G, Jo YS, Reichard KL, McFarland N, Chavkin C, Palmiter RD, et al. Synergy of Distinct Dopamine Projection Populations in Behavioral Reinforcement. Neuron. 2020 Mar;105(5):909-920.e5.

53. Cahill KM, Huo Z, Tseng GC, Logan RW, Seney ML. Improved identification of concordant and discordant gene expression signatures using an updated rank-rank hypergeometric overlap approach. Sci Rep. 2018 Jun 25;8(1):9588.

54. Plaisier SB, Taschereau R, Wong JA, Graeber TG. Rank–rank hypergeometric overlap: identification of statistically significant overlap between gene-expression signatures. Nucleic Acids Research. 2010 Sep;38(17):e169–e169.

55. Janky R, Verfaillie A, Imrichová H, Van De Sande B, Standaert L, Christiaens V, et al. iRegulon: From a Gene List to a Gene Regulatory Network Using Large Motif and Track Collections. Bussemaker HJ, editor. PLoS Comput Biol. 2014 Jul 24;10(7):e1003731.

56. Robison AJ, Nestler EJ. Transcriptional and epigenetic mechanisms of addiction. Nat Rev Neurosci. 2011 Nov;12(11):623–37.

57. Bali P, Kenny PJ. Transcriptional mechanisms of drug addiction. Dialogues in Clinical Neuroscience. 2019 Dec 31;21(4):379–87.

58. Calipari ES, Juarez B, Morel C, Walker DM, Cahill ME, Ribeiro E, et al. Dopaminergic dynamics underlying sex-specific cocaine reward. Nat Commun. 2017 Jan 10;8(1):13877.

59. Xu YT, Robson MJ, Szeszel-Fedorowicz W, Patel D, Rooney R, McCurdy CR, et al. CM156, a sigma receptor ligand, reverses cocaine-induced place conditioning and transcriptional responses in the brain. Pharmacology Biochemistry and Behavior. 2012 Mar;101(1):174–80.

60. Feng J, Wilkinson M, Liu X, Purushothaman I, Ferguson D, Vialou V, et al. Chronic cocaine-regulated epigenomic changes in mouse nucleus accumbens. Genome Biol. 2014 Apr 22;15(4):R65.

61. Navandar M, Martín-García E, Maldonado R, Lutz B, Gerber S, Ruiz De Azua I. Transcriptional signatures in prefrontal cortex confer vulnerability versus resilience to food and cocaine addiction-like behavior. Sci Rep. 2021 Apr 27;11(1):9076.

62. Winstanley CA, LaPlant Q, Theobald DEH, Green TA, Bachtell RK, Perrotti LI, et al. ΔFosB Induction in Orbitofrontal Cortex Mediates Tolerance to Cocaine-Induced Cognitive Dysfunction. J Neurosci. 2007 Sep 26;27(39):10497–507.

63. Lane DA, Lessard AA, Chan J, Colago EEO, Zhou Y, Schlussman SD, et al. Region-Specific Changes in the Subcellular Distribution of AMPA Receptor GluR1 Subunit in the Rat Ventral Tegmental Area after Acute or Chronic Morphine Administration. J Neurosci. 2008 Sep 24;28(39):9670–81.

64. Wang Y, Singh A, Li G, Yue S, Hertel K, Wang ZJ. Opioid induces increased DNA damage in prefrontal cortex and nucleus accumbens. Pharmacology Biochemistry and Behavior. 2023 Mar;224:173535.

65. Castel J, Li G, Onimus O, Leishman E, Cani PD, Bradshaw H, et al. NAPE-PLD in the ventral tegmental area regulates reward events, feeding and energy homeostasis. Mol Psychiatry. 2024 May;29(5):1478–90.

66. Fotio Y, Ciccocioppo R, Piomelli D. N-acylethanolamine acid amidase (NAAA) inhibition decreases the motivation for alcohol in Marchigian Sardinian alcohol-preferring rats. Psychopharmacology. 2021 Jan;238(1):249–58.

67. Yan Y, Peng C, Arvin MC, Jin XT, Kim VJ, Ramsey MD, et al. Nicotinic Cholinergic Receptors in VTA Glutamate Neurons Modulate Excitatory Transmission. Cell Reports. 2018 May;23(8):2236–44.

68. Li X, Xiong J, Zhang B, Zhangsun D, Luo S. α-Conotoxin TxIB Inhibits Development of Morphine-Induced Conditioned Place Preference in Mice via Blocking α6β2* Nicotinic Acetylcholine Receptors. Front Pharmacol. 2021 Dec 3;12:772990.

69. Dautan D, Souza AS, Huerta-Ocampo I, Valencia M, Assous M, Witten IB, et al. Segregated cholinergic transmission modulates dopamine neurons integrated in distinct functional circuits. Nat Neurosci. 2016 Aug;19(8):1025–33.

70. Pulipparacharuvil S, Renthal W, Hale CF, Taniguchi M, Xiao G, Kumar A, et al. Cocaine Regulates MEF2 to Control Synaptic and Behavioral Plasticity. Neuron. 2008 Aug;59(4):621–33.

71. Dieterich A, Floeder J, Stech K, Lee J, Srivastava P, Barker DJ, et al. Activation of Basolateral Amygdala to Nucleus Accumbens Projection Neurons Attenuates Chronic Corticosterone-Induced Behavioral Deficits in Male Mice. Front Behav Neurosci. 2021 Feb 24;15:643272.

72. Larson EB, Graham DL, Arzaga RR, Buzin N, Webb J, Green TA, et al. Overexpression of CREB in the Nucleus Accumbens Shell Increases Cocaine Reinforcement in Self-Administering Rats. J Neurosci. 2011 Nov 9;31(45):16447–57.

73. Carlezon WA, Thome J, Olson VG, Lane-Ladd SB, Brodkin ES, Hiroi N, et al. Regulation of Cocaine Reward by CREB. Science. 1998 Dec 18;282(5397):2272–5.

74. Brunzell DH, Mineur YS, Neve RL, Picciotto MR. Nucleus Accumbens CREB Activity is Necessary for Nicotine Conditioned Place Preference. Neuropsychopharmacol. 2009 Jul;34(8):1993–2001.

75. Misra K, Roy A, Pandey SC. Effects of voluntary ethanol intake on the expression of Ca2+/calmodulin-dependent protein kinase IV and on CREB expression and phosphorylation in the rat nucleus accumbens: Neuroreport. 2001 Dec;12(18):4133–7.

76. Guitart X, Thompson MA, Mirante CK, Greenberg ME, Nestler EJ. Regulation of Cyclic AMP Response Element-Binding Protein (CREB) Phosphorylation by Acute and Chronic Morphine in the Rat Locus Coeruleus. Journal of Neurochemistry. 1992 Mar;58(3):1168–71.

77. Nestler EJ, Tallman JF. Chronic morphine treatment increases cyclic AMP-dependent protein kinase activity in the rat locus coeruleus. Molecular Pharmacology. 1988;33(2):127–32.

78. Widnell KL, Self DW, Lane SB, Russell DS, Vaidya VA, Miserendino MJ, et al. Regulation of CREB expression: in vivo evidence for a functional role in morphine action in the nucleus accumbens. J Pharmacol Exp Ther. 1996 Jan;276(1):306–15.

79. Shinohara F, Kamii H, Minami M, Kaneda K. The Role of Dopaminergic Signaling in the Medial Prefrontal Cortex for the Expression of Cocaine-Induced Conditioned Place Preference in Rats. Biological & Pharmaceutical Bulletin. 2017;40(11):1983–9.

80. Hiroi N, White NM. The amphetamine conditioned place preference: differential involvement of dopamine receptor subtypes and two dopaminergic terminal areas. Brain Research. 1991 Jun;552(1):141–52.

81. O'Neal TJ, Bernstein MX, MacDougall DJ, Ferguson SM. A Conditioned Place Preference for Heroin Is Signaled by Increased Dopamine and Direct Pathway Activity and Decreased Indirect Pathway Activity in the Nucleus Accumbens. J Neurosci. 2022 Mar 9;42(10):2011–24.

82. Hnasko TS, Sotak BN, Palmiter RD. Morphine reward in dopamine-deficient mice. Nature. 2005 Dec;438(7069):854–7.

83. Hnasko TS, Sotak BN, Palmiter RD. Cocaine-Conditioned Place Preference by Dopamine-Deficient Mice Is Mediated by Serotonin. J Neurosci. 2007 Nov 14;27(46):12484–8.

84. Tervo DGR, Hwang BY, Viswanathan S, Gaj T, Lavzin M, Ritola KD, et al. A Designer AAV Variant Permits Efficient Retrograde Access to Projection Neurons. Neuron. 2016 Oct;92(2):372–82.

Figure Legends

Figure 1. **Chronic fentanyl induces discordant transcriptional adaptations between VTA-NAc and VTA-PFC neurons.** (**A**) Timeline for projection-specific VTA RNA sequencing experiments. Ribotag mice received retrograde Cre in either medial PFC or NAc core. Two weeks later, mice received 7 daily i.p. injections of 2 mg/kg fentanyl or equivalent volume of saline. Twenty-four hours after the last injection, brains were collected and fresh tissue punches containing VTA were flash frozen. Ribosome-associated RNA from VTA samples was isolated and prepared for RNA sequencing. (**B**) Heatmaps showing enrichment for neuron subtype markers and de-enrichment of non-neuronal markers in VTA-PFC or VTA-NAc saline samples vs saline input samples. (**C**) Heatmaps showing top five differentially expressed genes (DEGs) in fentanyl vs saline ($p<0.05$) across input, VTA-PFC, and VTA-NAc samples. (**C)** Alluvial plot comparing DEGs between neuronal populations. Combinations of upregulated (up), downregulated (down), and not significant (ns) genes are represented by individual colors. The 8 combinations with the most genes are in color, and the remaining combinations are represented in gray (**E**) RRHO interpretation schematic. (**F**) RRHO plots showing concordance of fentanyl-induced DEGs between total VTA and VTA-PFC, (**G**) concordance between total VTA and VTA-NAc, and (**H**) discordance between VTA-PFC and VTA-NAc, with $-\log_{10}$(P value) encoded in color using the adjacent color bars. (**I**) Circos plot showing WGCNA modules in VTA-NAc and (**J**) VTA-PFC pertaining to fentanyl, defined as differential eigengene expression with $p<0.05$ effect of fentanyl. Outer ring indicates an individual module assigned an arbitrary color and number. Fold change in eigengene expression and $-\log_{10}$(P value) are shown internally as sexes combined, then separately in females, and males, respectively. Hashed line on color bars indicates $p<0.05$ cut-offs.

Figure 2. DEG function and transcriptional regulators vary between VTA-NAc and VTA-PFC. (**A**) Gene ontology analysis of VTA-PFC fentanyl modules. Modules are sorted by upregulated (UP) vs downregulated (DOWN). Circle size represents number of genes in the module enriched for the GO term listed to the right. One significant GO term was chosen to represent each module. (**B**) Gene networks for select VTA-PFC fentanyl modules. Genes with the most connections (hub genes) are labelled and indicated by diamonds, with the size of the diamond scaled to the number of connections. (**C**) Gene ontology analysis of VTA-NAc fentanyl modules. (**D**) Gene networks for select VTA-NAc modules. (**E**) The top 5 predicted transcriptional regulators identified for select VTA-PFC fentanyl modules. Circle size represents the number of genes in the module that are regulated by the labeled transcription factor. (**F**) Regulatory network for *Creb1*, a transcriptional regulator of P43. Arrows point to genes from P43 that are regulatory targets of *Creb1*. The log fold change for each gene is represented in color. A representative enriched binding motif for *Creb1* is below. (**G**) The top 5 transcriptional regulators identified for select VTA-NAc fentanyl modules. (**H**) Regulatory network for *Mef2c*, a transcriptional regulator of N29, and representative binding motif is below.

Figure 3. VTA-NAc and VTA-PFC have elevated calcium activity in response to fentanyl exposure. (**A**) Timeline for projection-specific VTA GCaMP fiber photometry experiments. Mice received retrograde Cre in either the medial PFC or NAc core, and Cre-dependent GCaMP8s in VTA, with a fiber optic cannula implanted directly above VTA. Three weeks later, mice underwent fentanyl CPP and VTA GCaMP activity was recorded during all sessions. (**B**) Representative images depicting GCaMP expression in VTA-NAc and VTA-PFC with immunostaining for TH. Approximately 32.5% of VTA-NAc GCaMP neurons, and 28.4% of VTA-PFC GCaMP neurons, were TH positive (n=5 mice per group). (**C**) All mice spent more time in the fentanyl-paired context during the post-test compared to pre-test (n=10 mice per group; main effect of session, ****, $p<0.0001$) (**D**) Representative calcium traces from VTA-NAc (top) and VTA-PFC (bottom) during saline conditioning (left) and fentanyl conditioning (right). Ticks above the trace indicate identified calcium transients. (**E**) In VTA-NAc, fentanyl increases transient frequency (n=9, average over 3 conditioning days, **, $p=0.005$) (**F**) In VTA-PFC, fentanyl increases transient frequency (n=6, average over 3 conditioning days, **, $p=0.0099$). (**G**) During the post-test, VTA-NAc has reduced transient frequency when the mouse is in the fentanyl-paired compared to saline-paired context (n=10; *, $p=0.046$) (**H**) No difference in VTA-PFC transient frequency in saline-paired vs fentanyl-paired

context (n=10). Data are presented as mean±SEM with individual mice overlaid. Circles represent data points from females, triangles represent data points from males.

Figure 4. Temporally distinct calcium dynamics of VTA-NAc and VTA-PFC during fentanyl place preference. (**A**) Average zΔF/F for all VTA-NAc mice for 4 seconds surrounding the first 15 entries (left) or exits (right) to the saline-paired (gray trace) or fentanyl-paired (blue trace) context. Vertical dotted line represents the time of entry/exit. Using bootstrapped 95% confidence intervals, gray and blue horizontal bars represent where the gray and blue traces (saline-paired and fentanyl-paired, respectively) significantly differ from 0, and yellow shaded area represents where the two traces significantly differ from one another. (**B**) Heatmap of VTA-NAc activity for the 4 seconds surrounding the first 15 entries into the fentanyl-paired region. Color represents zΔF/F averaged across all VTA-NAc mice. (**C-D**) Same as A-B, but for VTA-PFC. During the pre-test for (**E**) VTA-NAc and (**F**) VTA-PFC, there is no difference in mean zΔF/F from -2 to -1 seconds (left) or -1 to 0 seconds (right) preceding entry to either context. (**G**) During the post-test for VTA-NAc, there is greater calcium activity from -1 to 0 second preceding entries to fentanyl-paired vs saline-paired context (n=10; *, p=0.04). (**H**) During post-test for VTA-PFC, there is a trend towards increased mean zΔF/F during entries to fentanyl-paired context at both -2 to -1, and -1 to 0 (n=10). Data are presented as mean±SEM with individual mice overlaid. Circles represent data points from females and triangles represent data points from males.

Figure 5. Chemogenetic inhibition of VTA-NAc vs VTA-PFC differentially impacts fentanyl place preference. (**A**) Timeline for chemogenetic experiments. Mice received retrograde-Cre in either medial PFC or NAc core, and Cre-dependent hM4Gi, or Cre-dependent mCherry, in VTA. Twenty minutes prior to each post-test, mice received DCZ (0.1 mg/kg i.p.) or vehicle in a counterbalanced within-subject design. (**B**) Time spent in fentanyl-paired context (*, p=0.012), (**C**) number of entries to fentanyl-paired context, (**D**) number of entries to the saline-paired context, and (**E**) total movement counts after treatment with vehicle (gray) and DCZ (light blue) in mice expressing mCherry or hM4Gi in VTA-NAc. (**F**) Time spent in fentanyl-paired context, (**G**) number of entries to fentanyl-paired context (*, p=0.046), (**H**) number of entries to the saline-paired context, and (**I**) total movement counts (*, p=0.028) after treatment with vehicle (gray) and DCZ (dark blue) in mice expressing

mCherry or hM4Gi in VTA-PFC. Data are presented as mean±SEM with individual mice overlaid. Circles represent data points from females and triangles represent data points from males. N=11-12 per group.

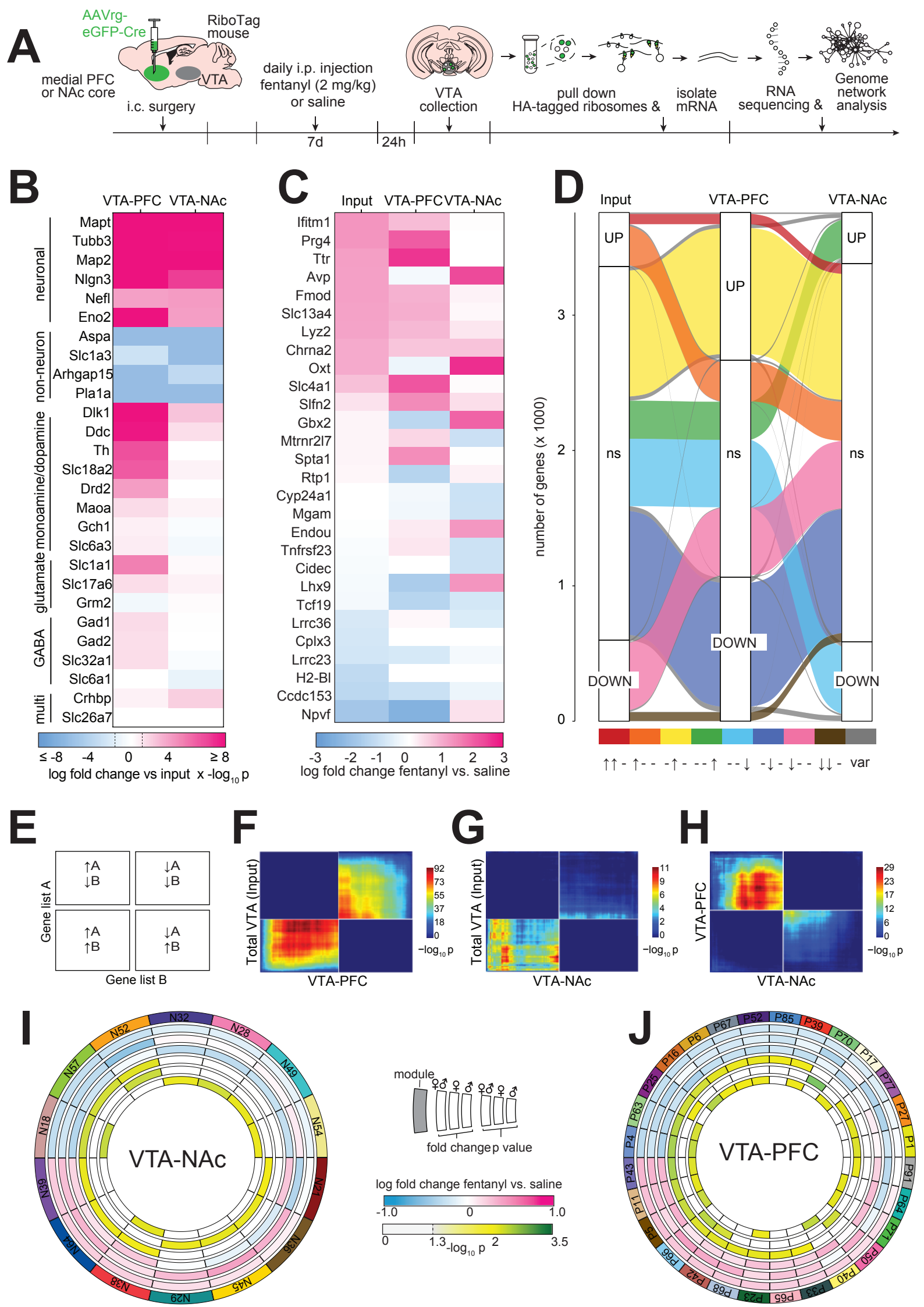
A
AAVrg-eGFP-Cre
RiboTag mouse
medial PFC or NAc core
VTA
i.c. surgery
daily i.p. injection fentanyl (2 mg/kg) or saline
7d
24h
VTA collection
pull down HA-tagged ribosomes &
isolate mRNA
RNA sequencing &
Genome network analysis
B
VTA-PFC VTA-NAc
neuronal
non-neuron
monoamine/dopamine
glutamate
GABA
multi
Mapt
Tubb3
Map2
Nlgn3
Nefl
Eno2
Aspa
Slc1a3
Arhgap15
Pla1a
Dlk1
Ddc
Th
Slc18a2
Drd2
Maoa
Gch1
Slc6a3
Slc1a1
Slc17a6
Grm2
Gad1
Gad2
Slc32a1
Slc6a1
Crhbp
Slc26a7
≤ -8 -4 0 4 ≥ 8
log fold change vs input x -log10 p
C
Input VTA-PFC VTA-NAc
Ifitm1
Prg4
Ttr
Avp
Fmod
Slc13a4
Lyz2
Chrna2
Oxt
Slc4a1
Slfn2
Gbx2
Mtrnr2l7
Spta1
Rtp1
Cyp24a1
Mgam
Endou
Tnfrsf23
Cidec
Lhx9
Tcf19
Lrrc36
Cplx3
Lrrc23
H2-Bl
Ccdc153
Npvf
-3 -2 -1 0 1 2 3
log fold change fentanyl vs. saline
D
Input VTA-PFC VTA-NAc
UP
ns
DOWN
number of genes (x 1000)
0 1 2 3
↑↑ - ↑- - -↑- - - -↑ - -↓ -↓- ↓- - ↓↓ - var
E
Gene list A
Gene list B
↑A ↓B
↓A ↓B
↑A ↑B
↓A ↑B
F
Total VTA (Input)
VTA-PFC
92 73 55 37 18 0
−log10 p
G
Total VTA (Input)
VTA-NAc
11 9 6 4 2 0
−log10 p
H
VTA-PFC
VTA-NAc
29 23 17 12 6 0
−log10 p
I
VTA-NAc
N32 N28 N49 N54 N21 N36 N45 N29 N38 N64 N69 N18 N57 N52
module
fold change p value
log fold change fentanyl vs. saline
-1.0 0 1.0
0 1.3 2 3.5
-log10 p
J
VTA-PFC
P85 P39 P70 P17 P77 P27 P1 P61 P84 P71 P50 P40 P33 P65 P23 P68 P42 P66 P9 P11 P43 P4 P63 P25 P16 P6 P67 P52

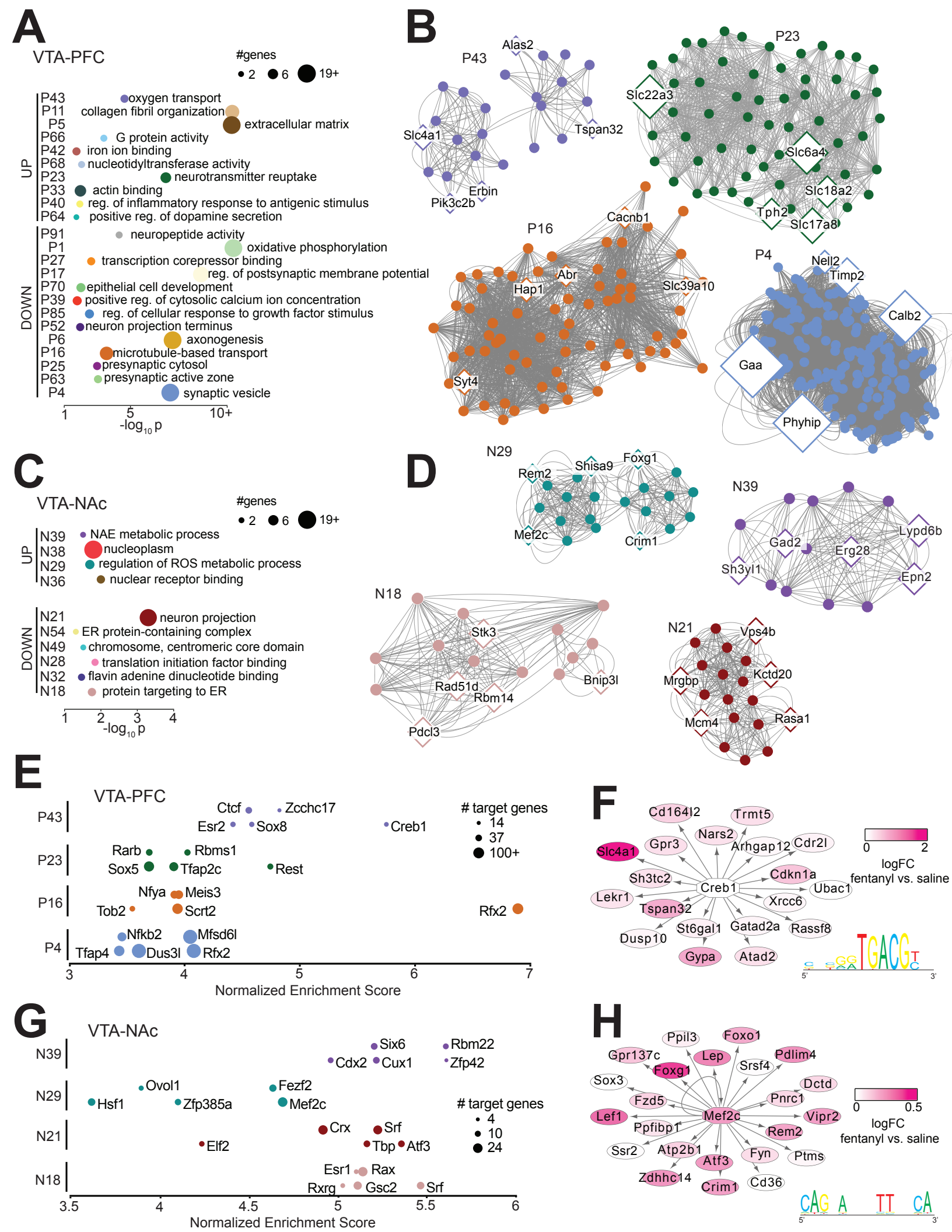
A
VTA-PFC
#genes
2
6
19+
UP
P43 oxygen transport
P11 collagen fibril organization
P5 extracellular matrix
P66 G protein activity
P42 iron ion binding
P68 nucleotidyltransferase activity
P23 neurotransmitter reuptake
P33 actin binding
P40 reg. of inflammatory response to antigenic stimulus
P64 positive reg. of dopamine secretion
DOWN
P91 neuropeptide activity
P1 oxidative phosphorylation
P27 transcription corepressor binding
P17 reg. of postsynaptic membrane potential
P70 epithelial cell development
P39 positive reg. of cytosolic calcium ion concentration
P85 reg. of cellular response to growth factor stimulus
P52 neuron projection terminus
P6 axonogenesis
P16 microtubule-based transport
P25 presynaptic cytosol
P63 presynaptic active zone
P4 synaptic vesicle
1
5
10+
-log10 p
B
P43
Alas2
Slc4a1
Tspan32
Erbin
Pik3c2b
P23
Slc22a3
Slc6a4
Slc18a2
Tph2
Slc17a8
P16
Cacnb1
Abr
Hap1
Slc39a10
Syt4
P4
Nell2
Timp2
Calb2
Gaa
Phyhip
C
VTA-NAc
#genes
2
6
19+
UP
N39 NAE metabolic process
N38 nucleoplasm
N29 regulation of ROS metabolic process
N36 nuclear receptor binding
DOWN
N21 neuron projection
N54 ER protein-containing complex
N49 chromosome, centromeric core domain
N28 translation initiation factor binding
N32 flavin adenine dinucleotide binding
N18 protein targeting to ER
1
2
3
4
-log10 p
D
N29
Rem2
Shisa9
Foxg1
Mef2c
Crim1
N39
Gad2
Erg28
Lypd6b
Sh3yl1
Epn2
N18
Stk3
Rad51d
Rbm14
Bnip3l
Pdcl3
N21
Vps4b
Mrgbp
Kctd20
Mcm4
Rasa1
E
VTA-PFC
P43
Ctcf
Zcchc17
Esr2
Sox8
Creb1
P23
Rarb
Rbms1
Sox5
Tfap2c
Rest
P16
Nfya
Meis3
Tob2
Scrt2
Rfx2
P4
Nfkb2
Mfsd6l
Tfap4
Dus3l
Rfx2
target genes
14
37
100+
3
4
5
6
7
Normalized Enrichment Score
F
Cd164l2
Trmt5
Nars2
Gpr3
Arhgap12
Cdr2l
Slc4a1
Sh3tc2
Cdkn1a
Creb1
Ubac1
Lekr1
Xrcc6
Tspan32
Dusp10
St6gal1
Gatad2a
Rassf8
Gypa
Atad2
0
2
logFC
fentanyl vs. saline
5'
3'
G
VTA-NAc
N39
Six6
Rbm22
Cdx2
Cux1
Zfp42
N29
Ovol1
Fezf2
Hsf1
Zfp385a
Mef2c
N21
Crx
Srf
Elf2
Tbp
Atf3
N18
Esr1
Rax
Rxrg
Gsc2
Srf
target genes
4
10
24
3.5
4
4.5
5
5.5
6
Normalized Enrichment Score
H
Ppil3
Foxo1
Gpr137c
Lep
Pdlim4
Foxg1
Srsf4
Sox3
Dctd
Fzd5
Pnrc1
Lef1
Mef2c
Vipr2
Ppfibp1
Rem2
Ssr2
Atp2b1
Fyn
Ptms
Atf3
Zdhhc14
Crim1
Cd36
0
0.5
logFC
fentanyl vs. saline
5'
3'

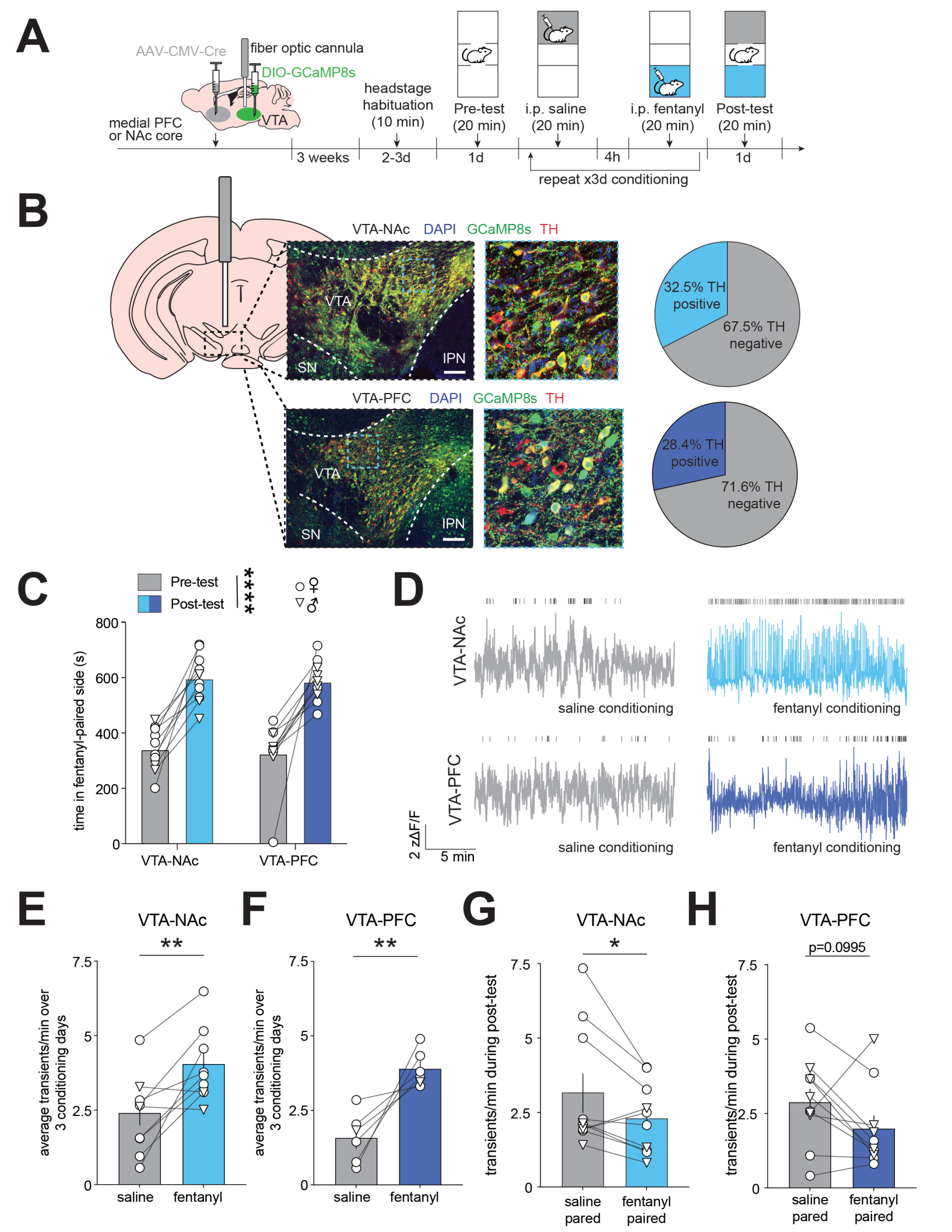
A
AAV-CMV-Cre
fiber optic cannula
DIO-GCaMP8s
VTA
medial PFC
or NAc core
headstage
habituation
(10 min)
Pre-test
(20 min)
i.p. saline
(20 min)
i.p. fentanyl
(20 min)
Post-test
(20 min)
3 weeks
2-3d
1d
4h
1d
repeat x3d conditioning
B
VTA-NAc DAPI GCaMP8s TH
VTA
SN
IPN
32.5% TH positive
67.5% TH negative
VTA-PFC DAPI GCaMP8s TH
28.4% TH positive
71.6% TH negative
C
Pre-test
Post-test
****
time in fentanyl-paired side (s)
VTA-NAc
VTA-PFC
D
VTA-NAc
VTA-PFC
saline conditioning
fentanyl conditioning
2 zΔF/F
5 min
E
VTA-NAc
average transients/min over 3 conditioning days
saline
fentanyl
F
VTA-PFC
G
VTA-NAc
transients/min during post-test
saline pared
fentanyl paired
H
VTA-PFC
p=0.0995

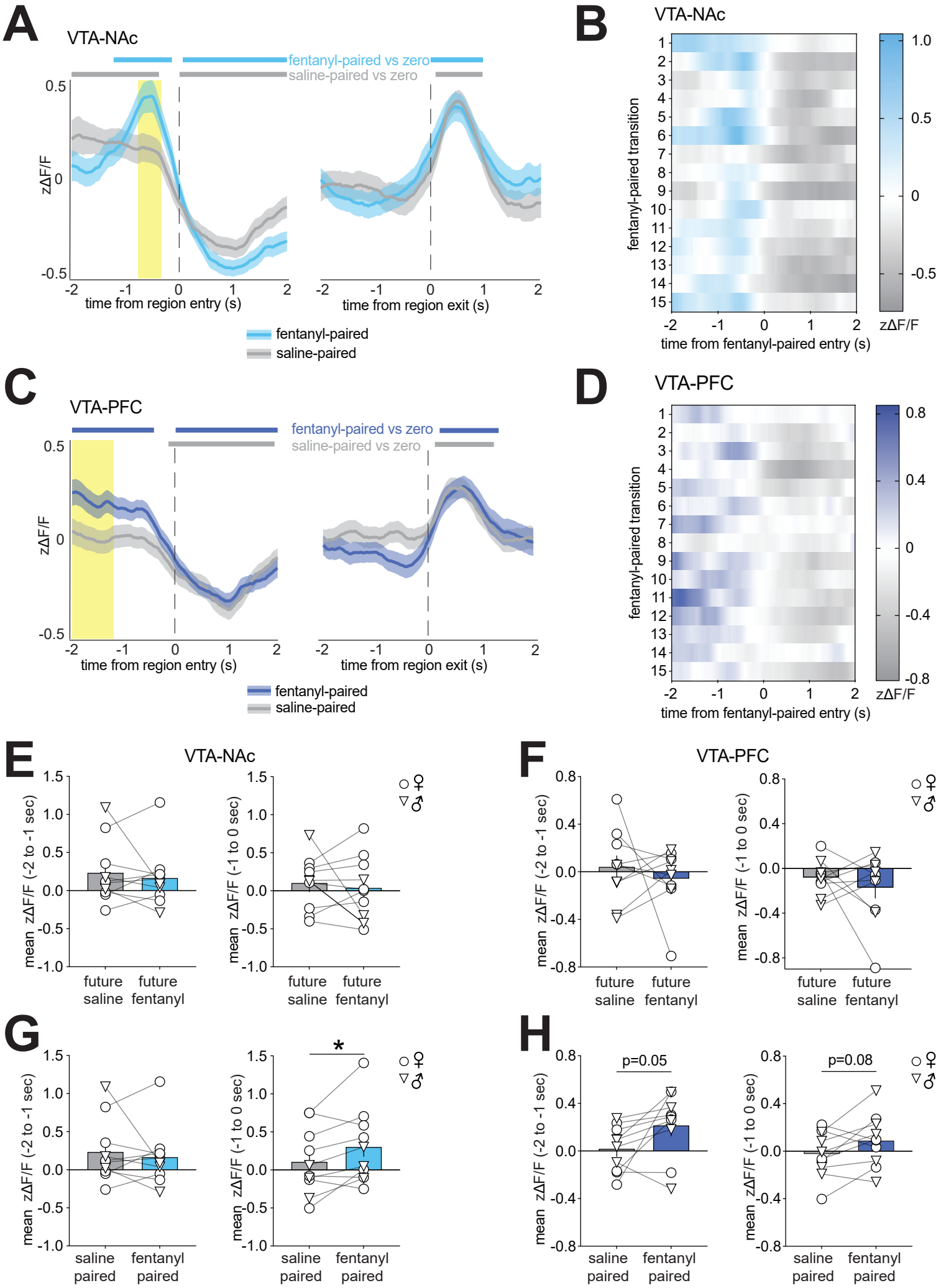
A
VTA-NAc
fentanyl-paired vs zero
saline-paired vs zero
zΔF/F
time from region entry (s)
time from region exit (s)
fentanyl-paired
saline-paired
B
VTA-NAc
fentanyl-paired transition
time from fentanyl-paired entry (s)
zΔF/F
C
VTA-PFC
fentanyl-paired vs zero
saline-paired vs zero
zΔF/F
time from region entry (s)
time from region exit (s)
fentanyl-paired
saline-paired
D
VTA-PFC
fentanyl-paired transition
time from fentanyl-paired entry (s)
zΔF/F
E
VTA-NAc
mean zΔF/F (-2 to -1 sec)
mean zΔF/F (-1 to 0 sec)
future saline
future fentanyl
F
VTA-PFC
mean zΔF/F (-2 to -1 sec)
mean zΔF/F (-1 to 0 sec)
future saline
future fentanyl
G
mean zΔF/F (-2 to -1 sec)
mean zΔF/F (-1 to 0 sec)
*
saline paired
fentanyl paired
H
p=0.05
p=0.08
mean zΔF/F (-2 to -1 sec)
mean zΔF/F (-1 to 0 sec)
saline paired
fentanyl paired

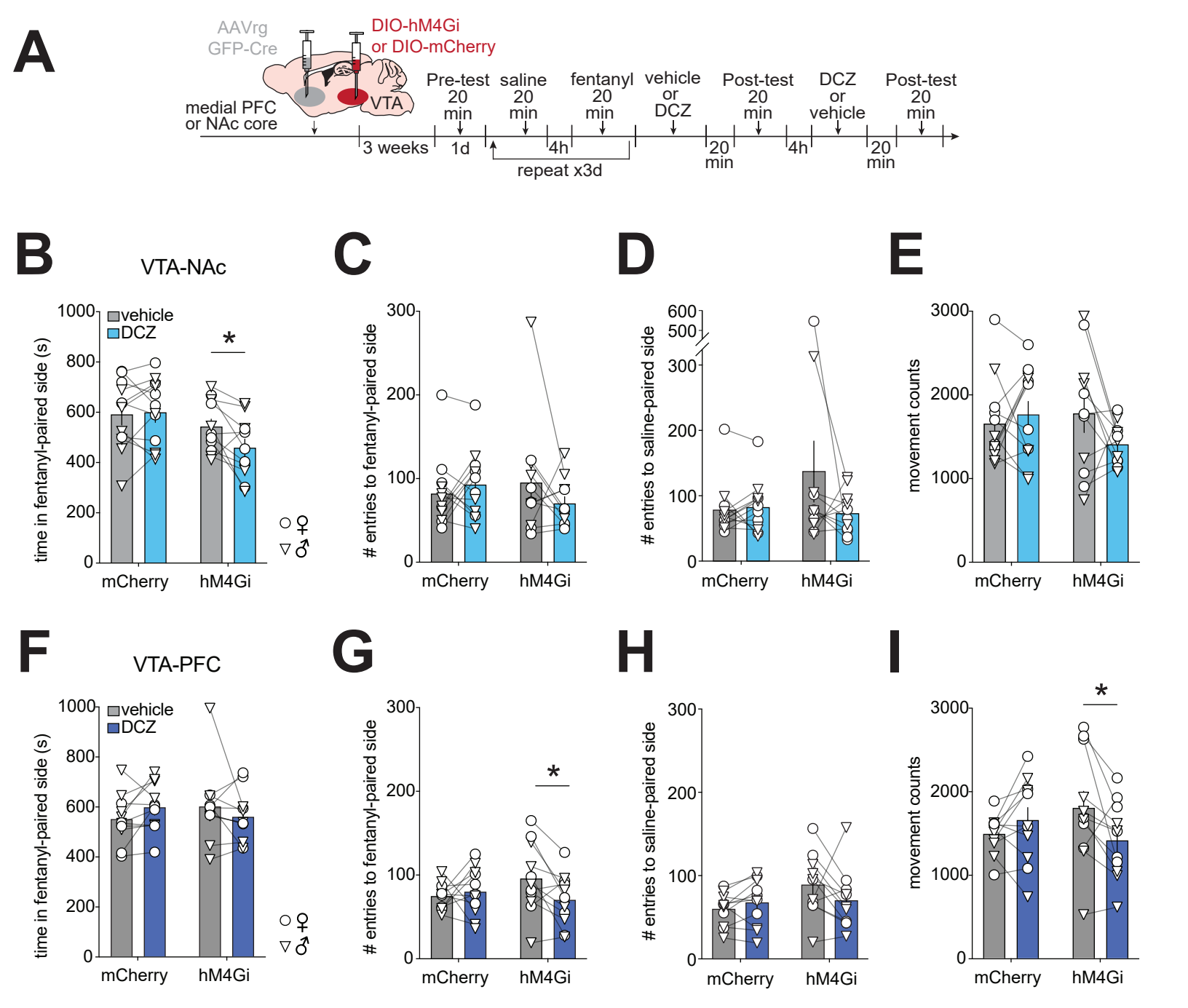
A
AAVrg
GFP-Cre
DIO-hM4Gi
or DIO-mCherry
medial PFC
or NAc core
VTA
Pre-test
20
min
saline
20
min
fentanyl
20
min
vehicle
or
DCZ
Post-test
20
min
DCZ
or
vehicle
Post-test
20
min
3 weeks
1d
4h
repeat x3d
20
min
4h
20
min
B
VTA-NAc
vehicle
DCZ
time in fentanyl-paired side (s)
mCherry
hM4Gi
C
entries to fentanyl-paired side
D
entries to saline-paired side
E
movement counts
F
VTA-PFC
G
H
I